Electronic Supplementary Information

A universal strategy to high redox-active porous carbons for efficient energy storage

Ziyang Song,[a] Ling Miao,[a] Liangchun Li,[a] Dazhang Zhu,[a] Yaokang Lv,[b] Wei Xiong,[c] Hui Duan,[a] Zhiwei Wang,[d] Lihua Gan[a] and Mingxian Liu*[ade]

[a]Shanghai Key Lab of Chemical Assessment and Sustainability, School of Chemical Science and Engineering, Tongji University, Shanghai, 200092, P. R. China.

[b]College of Chemical Engineering, Zhejiang University of Technology, Hangzhou 310014, P. R. China.

[c]School of Chemistry and Environmental Engineering, Key Laboratory for Green Chemical Process (Ministry of Education), Hubei Key Lab of Novel Reactor & Green Chemical Technology, Wuhan Institute of Technology, Liufang Road 1, Wuhan, 430205, P. R. China

[d]State Key Laboratory of Pollution Control and Resources Reuse, Shanghai Institute of Pollution Control and Ecological Security, School of Environmental Science and Engineering, Tongji University, Shanghai 200092, P. R. China.

[e]College of Chemistry and Molecular Engineering, Zhengzhou University, Zhengzhou 450001, P. R. China.

Corresponding Author

*E-mail: liumx@tongji.edu.cn.

Experimental section

Synthesis. A homogeneous solution composed of 0.06 mol benzoquinone (BQ, 6.48 g), 0.02 mol amine (*o*-phenylenediamine (PD, 2.16 g), ethylenediamine (ED, 1.20 g), 1,5-diaminonaphthalene (DN, 3.16 g) and 1,4-cyclohexanediamine (CD, 2.28 g)), and 200 mL ethanol was stirred at 50 ℃ for 2 h to synthesize polymer BQ/PD, BQ/ED, BQ/DN and BQ/CD, respectively. After filtering, washing and drying, the collected polymer was mixed with KOH (1:1, w/w), and subsequently heated to 750 ℃ for 2 h under N_2 flow to obtain high redox-active carbon-based materials, denoted as BQ/PD-C, BQ/ED-C, BQ/DN-C and BQ/CD-C, respectively.

Characterization. The microcosmic structures of the samples were observed by scanning electron microscopy (SEM, Hitachi S-4800) and transmission electron microscopy (TEM, JEM-2100). Fourier transform infrared spectroscopy (FT-IR) was performed using a Thermo Nicolet NEXUS spectrometer. Thermogravimetric analysis of the samples was conducted using a Netzsch STA409 PC analyzer at a heating rate 10 ℃ min^{-1} under an N_2 atmosphere. The N_2 adsorption/desorption isotherms were evaluated at −196 ℃ on a Micromeritics ASAP 2460 apparatus. The surface area was acquired by Braunauer–Emmett–Teller method. The pore size distribution was estimated using nitrogen desorption branches of the isotherms by the nonlocal density functional theory equilibrium model for slit pores. X-ray photoelectron spectroscopy (XPS) tests were conducted by an AXIS Ultra DLD X-ray photoelectron system with Al Ka radiation to investigate the surface functionality. Ultraviolet visible near infrared (UV−vis−NIR) spectra were obtained using an Agilent Carry 5000 spectrometer.

Assembly of supercapacitors. The working electrode was assembled by a mixture of the prepared carbon, graphite and polytetrafluoroethylene with a weight ratio of 8:1:1. The mixture

was dispersed in ethanol to obtain a homogeneous slurry and followed dried at 80 ℃ overnight, after that, pressed the resultant dough onto the stainless steel mesh (mass loading of electroactive materials: ~10 mg cm^{-2}) under 20 MPa. To construct symmetric supercapacitors, two same working electrodes were packed in a 2016-type coin cell together with a polypropylene membrane separator (Celgard 3501) and 100 μL electrolytes of H_2SO_4 (1 M), KOH (6 M), Na_2SO_4 (1 M), lithium bis(trifluoromethane sulfonyl)imide (LiTFSI) solution (7 m, mol salt in kg-solvent), and ionic liquid of 1-ethyl-3-methylimidazolium tetrafluoroborate ($EMIMBF_4$), respectively.

Electrochemical measurement. A CHI660E electrochemical workstation was used to analyze the electrochemical behaviors of obtained samples including cyclic voltammetry (CV), galvanostatic charge–discharge (GCD), and electrochemical impedance spectroscopy (EIS). The gravimetric capacitance (C_s) of single electrode, energy density (E) and power density (P) of the devices were calculated according to the following equations:

$$C_s\,(\mathrm{F\ g^{-1}}) = \frac{4 \times I \times \Delta t}{m \times \Delta V} \tag{1}$$

$$C_v\,(\mathrm{F\ cm^{-3}}) = \rho \times C_s = (V_t + 1/\rho_{carbon})^{-1} \times C_s \tag{2}$$

$$E\,(\mathrm{Wh\ kg^{-1}}) = \frac{1}{7.2 \times 4} C_s \Delta V^2 \tag{3}$$

$$E_v\,(\mathrm{Wh\ L^{-1}}) = \rho \times E \tag{4}$$

$$P\,(\mathrm{W\ kg^{-1}}) = \frac{E}{\Delta t} \times 3600 \tag{5}$$

$$P_v\,(\mathrm{W\ L^{-1}}) = \rho \times P \tag{6}$$

I (A): charge current; Δt (s): discharge time; m (g): the total mass of active material on two electrodes; ΔV (V): the voltage window; C_v is the volumetric capacitance of one electrode; ρ is the packing density of carbon material; V_t denotes the total pore volume of carbon material, and ρ_{carbon} is the true density of carbon (2 g cm^{-3}). E_v and P_v represents the volumetric energy and power density of the symmetrical devices, respectively.

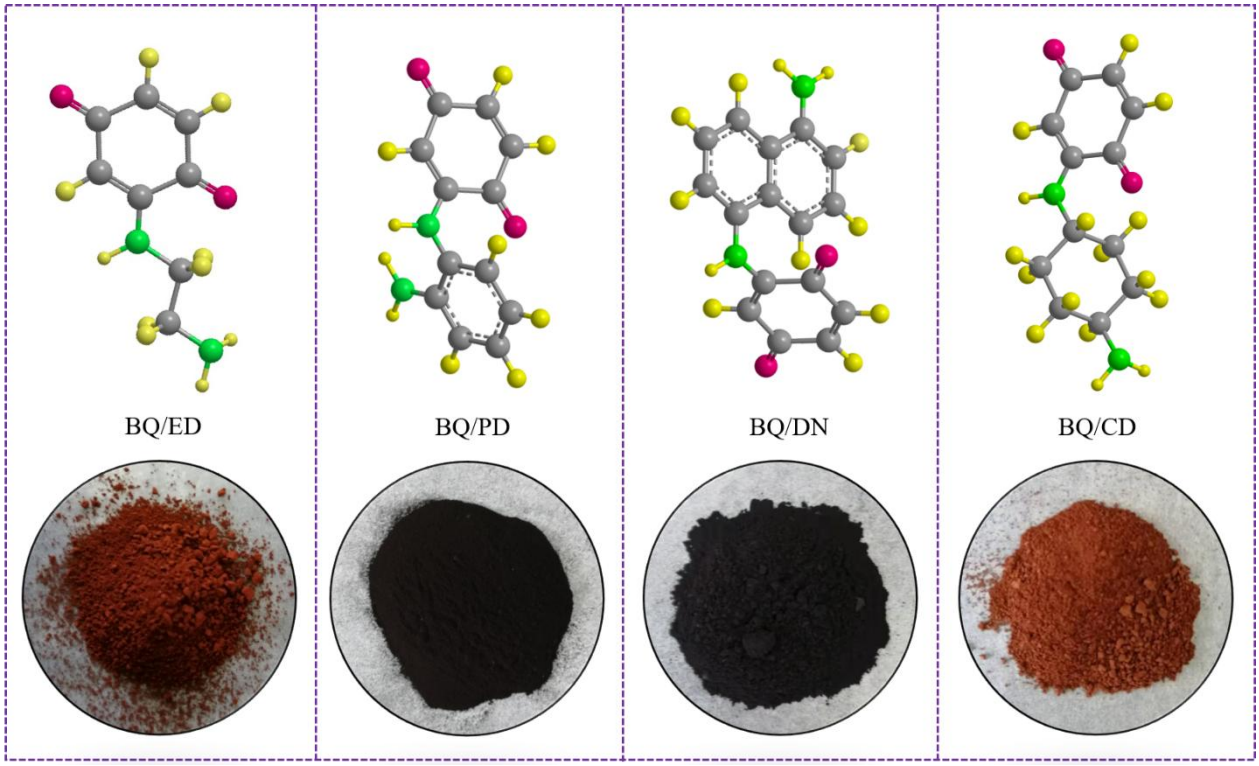

Fig. S1 Three-dimensional unit networks and photographs of the BQ/*X* polymers.

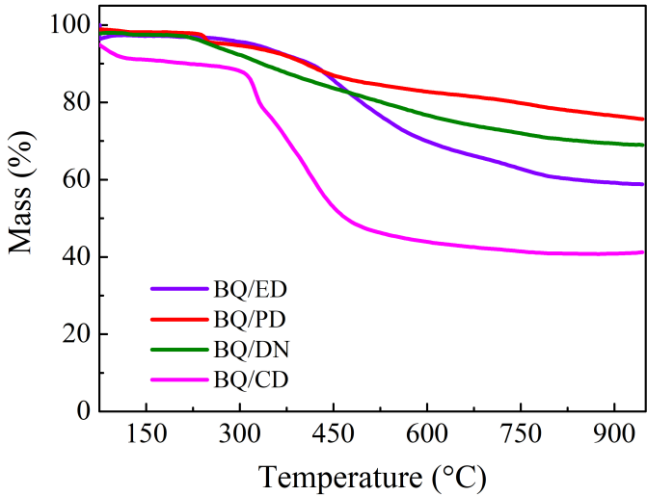

Fig. S2 TGA scans of the BQ/*X* polymers.

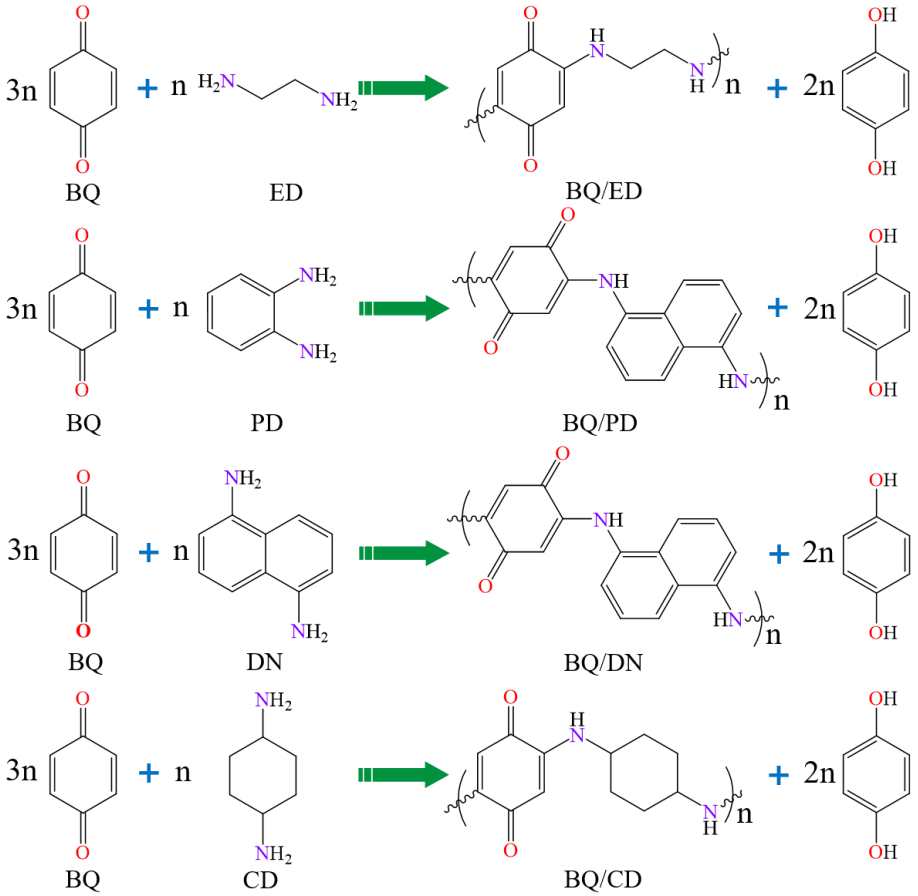

Fig. S3 Reaction process of benzoquinone and various amines in ethanol.

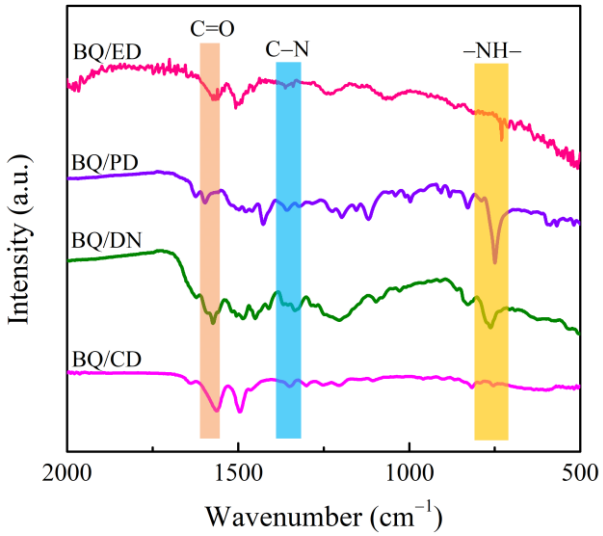

Fig. S4 IR spectra of the BQ/*X* polymers.

Calculation of Hansen solubility parameters of BQ/*X* polymers.

The Hansen solubility parameters (defined as δ) of BQ/*X* polymers was experimentally evaluated by the dissolution approach according to the literature,[1, 2] which were obtained as solubility parameters associated with the solvent that show the highest dispersion concentration. Specifically, BQ/*X* polymers were dispersed into thirteen different solvents with known δ respectively. The obtained dispersions were allowed to stand for one day, and the concentrations of BQ/*X* in the supernatant of the dispersions were then obtained by the Beer-Lambert-Bouguer law based on measured absorbance at 343 nm, which was the maximum absorbance of BQ/*X*. Through this process, the equilibrium concentrations of BQ/*X* in each of the thirteen solutions with different δ could be obtained. The concentration was plotted versus the solubility parameters. Based on this method, the δ of BQ/*X* were experimentally determined in **Fig. S5**. The δ values of BQ/ED, BQ/PD, BQ/DN and BQ/CD were estimated to be found as 25.3, 26.2, 24.9, and 24.4 $(Mpa)^{1/2}$, respectively (**Table S1**).

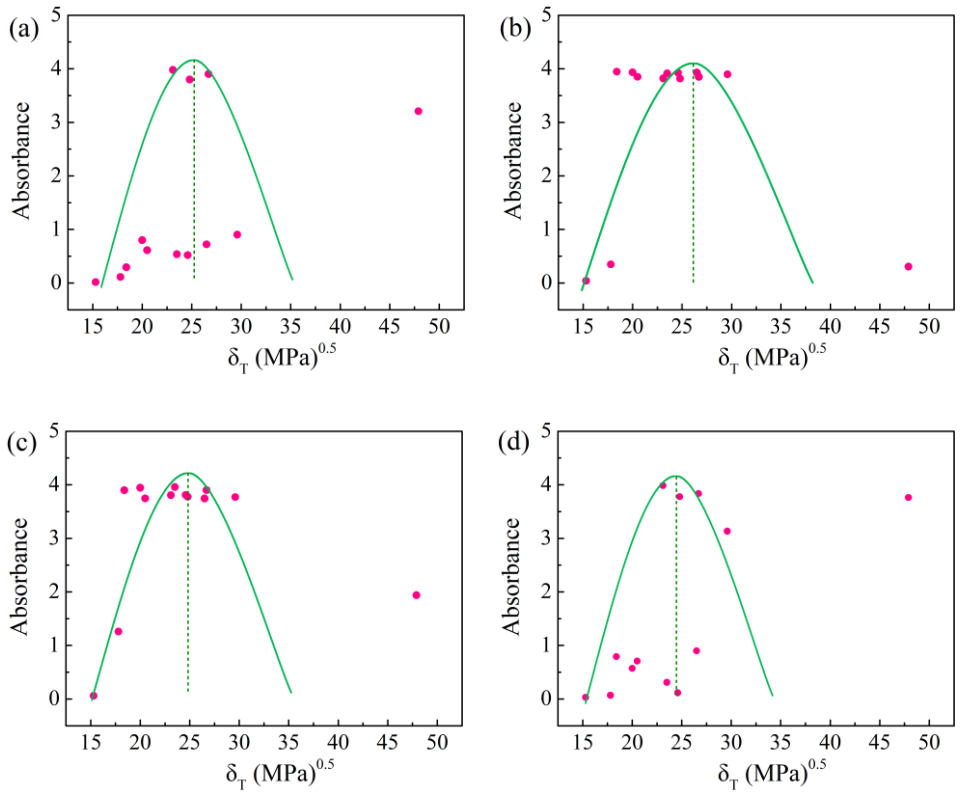

Fig. S5 The concentration of BQ/*X* polymers analysed with UV vis plotted with HSP of solvent (the dotted lines were provided to highlight the maximum absorption peaks and corresponding abscissa values).

Table S1. Hansen solubility parameters of thirteen solvents and four polymers in this work.[3]

Order	Solvent/Polymer	δ	Order	Solvent/Polymer	δ
1	Hexane	15.3	10	Ethanol	26.5
2	Trimethylbenzene	17.8	11	Dimethyl sulfoxide	26.7
3	Dichloroethane	18.4	12	Methanol	29.6
4	Acetone	20	13	Water	47.9
5	Dioxane	20.5	14	BQ/ED	25.3
6	N-methylpyrrolidone	23.1	15	BQ/PD	26.2
7	Isopropanol	23.5	16	BQ/DN	24.9
8	Acetonitrile	24.6	17	BQ/CD	24.4

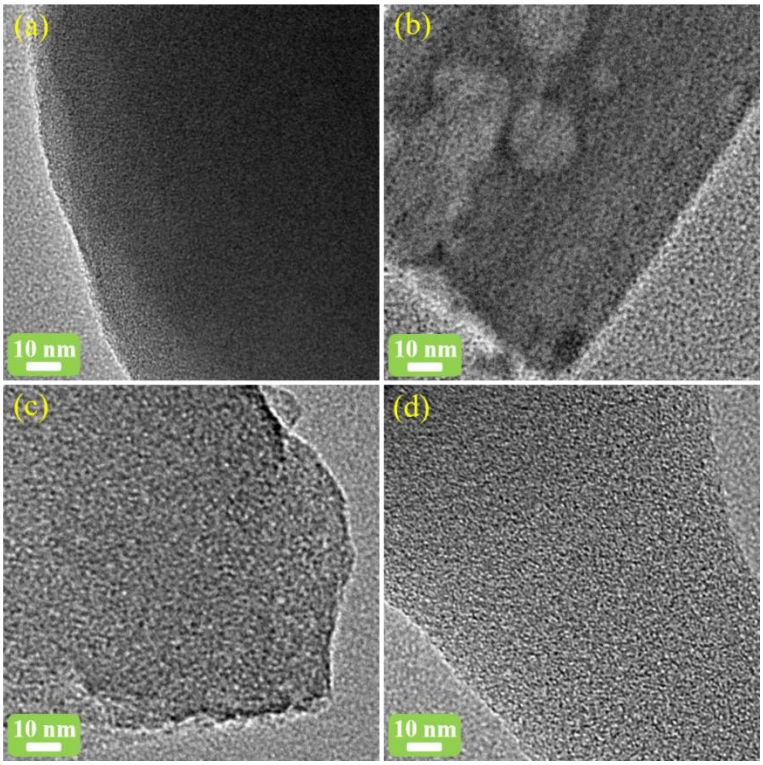

Fig. S6 HRTEM images for (a) BQ/ED-C, (b) BQ/PD-C, (c) BQ/DN-C, and (d) BQ/CD-C.

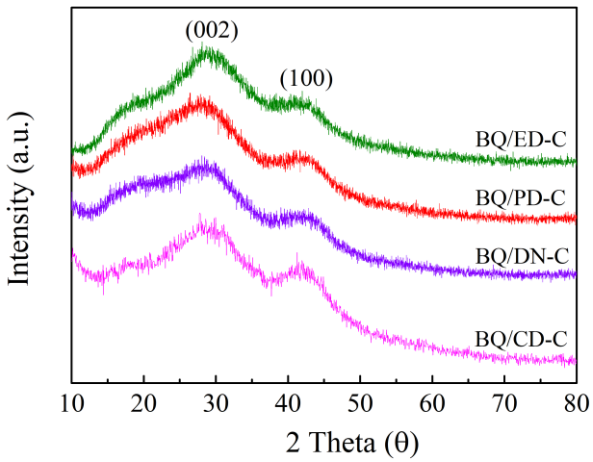

Fig. S7 XRD patterns of BQ/*X*-C.

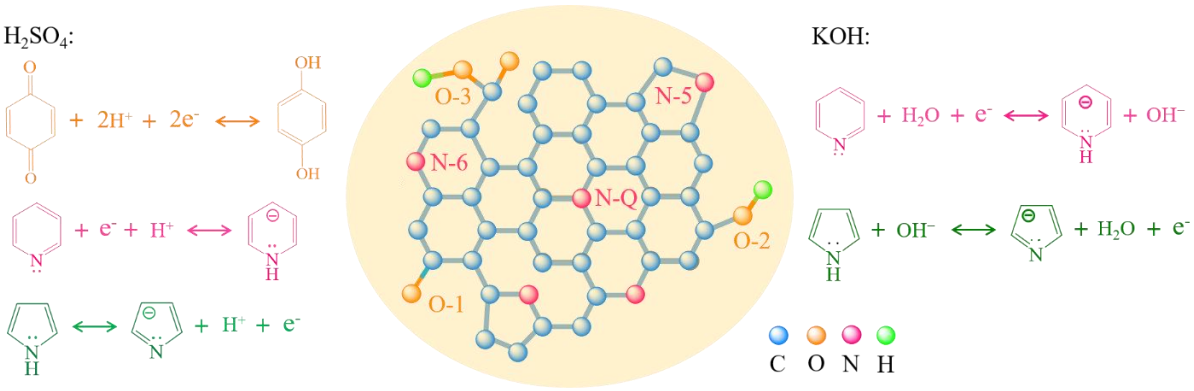

Fig. S8 The locations of heteroatoms in the carbon matrix and corresponding redox reactions.

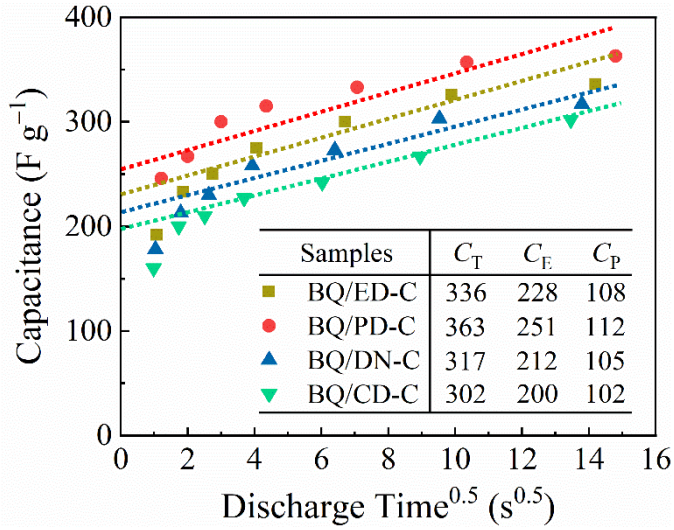

Fig. S9 The capacitance *vs*. square root of half-cycle time.

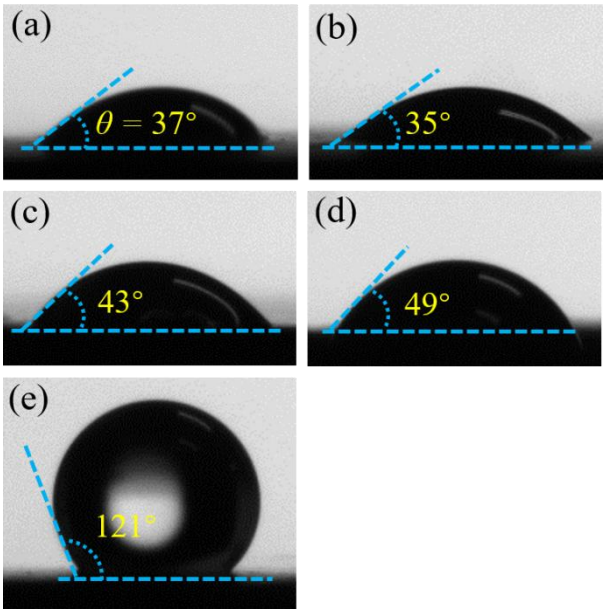

Fig. S10 The water contact angle (θ) measurements of (a) BQ/ED-C, (b) BQ/PD-C, (c) BQ/DN-C, (d) BQ/CD-C, and (e) commercial activate carbon.

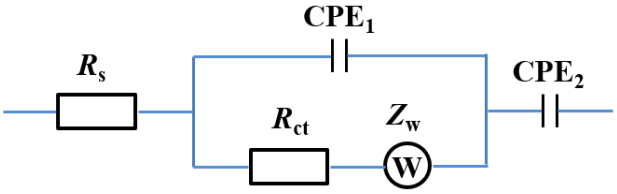

Fig. S11 The model of Nyquist plots.

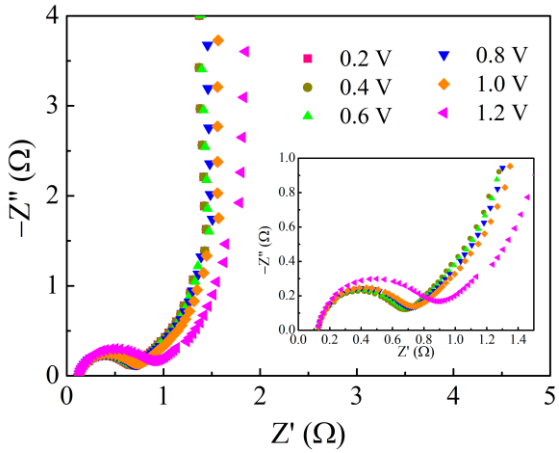

Fig. S12 Nyquist plots measured at different potentials.

Table S2. The comparison of parameters related to ion diffusion of the samples.

Devices	R_s (Ω)	R_{ct} (Ω)	τ (s)	σ (Ω $s^{-0.5}$)	D_{H^+} (cm^2 s^{-1})
BQ/ED-C	0.14	0.64	1.01	0.97	1.53×10^{-8}
BQ/PD-C	0.13	0.41	0.59	0.34	1.24×10^{-7}
BQ/DN-C	0.15	0.95	1.09	1.10	1.19×10^{-8}
BQ/CD-C	0.18	0.88	1.48	1.16	1.07×10^{-8}

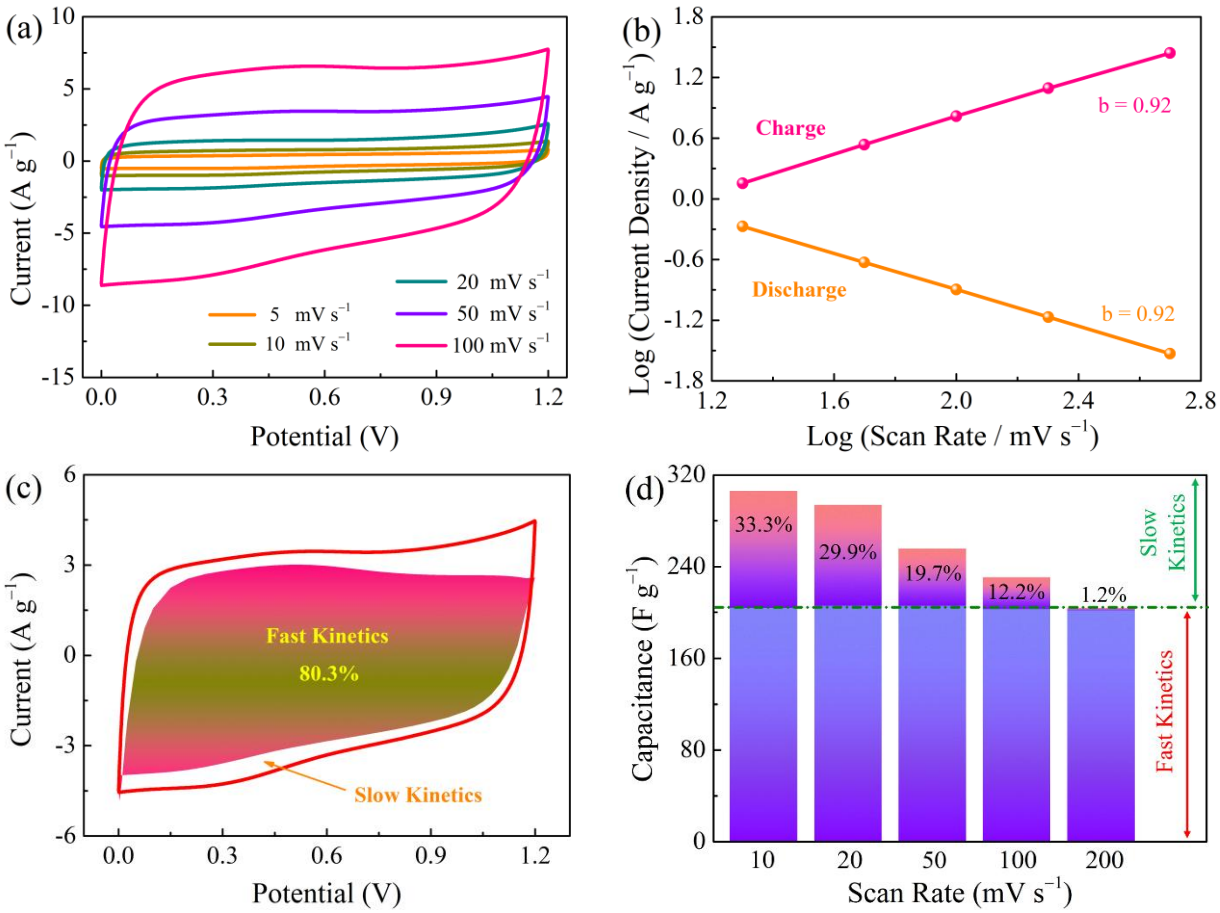

Fig. S13 (a) CV curves at various scan rates, (b) Absolute current density and scan rate obey the power law, $i=kv^b$, in charge/discharge process, (c) Decoupling of the capacitance contributed by the fast-kinetic process (shadow) and the slow-kinetic processes (blank), (d) Histograms of the capacitance contribution from fast and slow kinetic process of BQ/ED-C supercapacitor.

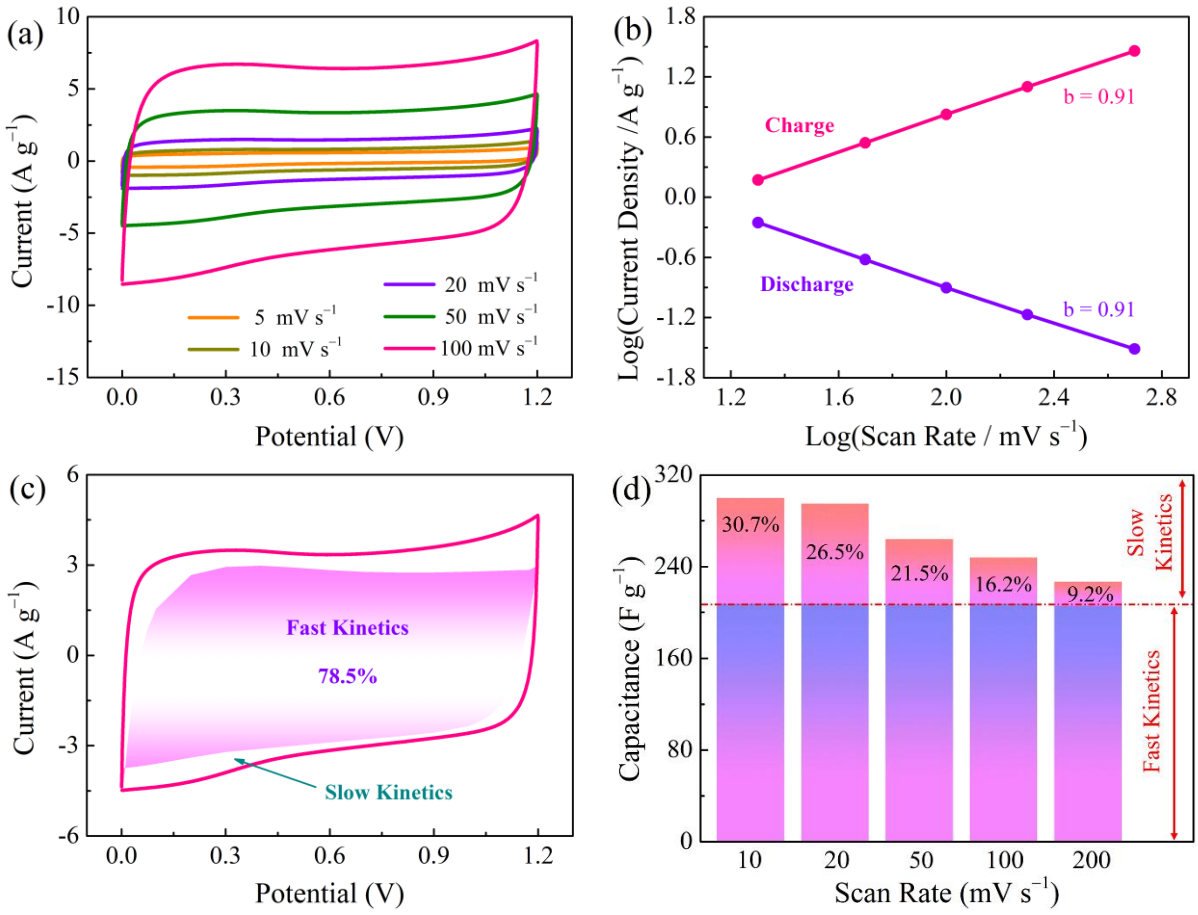

Fig. S14 (a) CV curves at various scan rates, (b) Absolute current density and scan rate obey the power law, $i=kv^b$, in charge/discharge process, (c) Decoupling of the capacitance contributed by the fast-kinetic process (shadow) and the slow-kinetic processes (blank), (d) Histograms of the capacitance contribution from fast and slow kinetic process of BQ/DN-C supercapacitor.

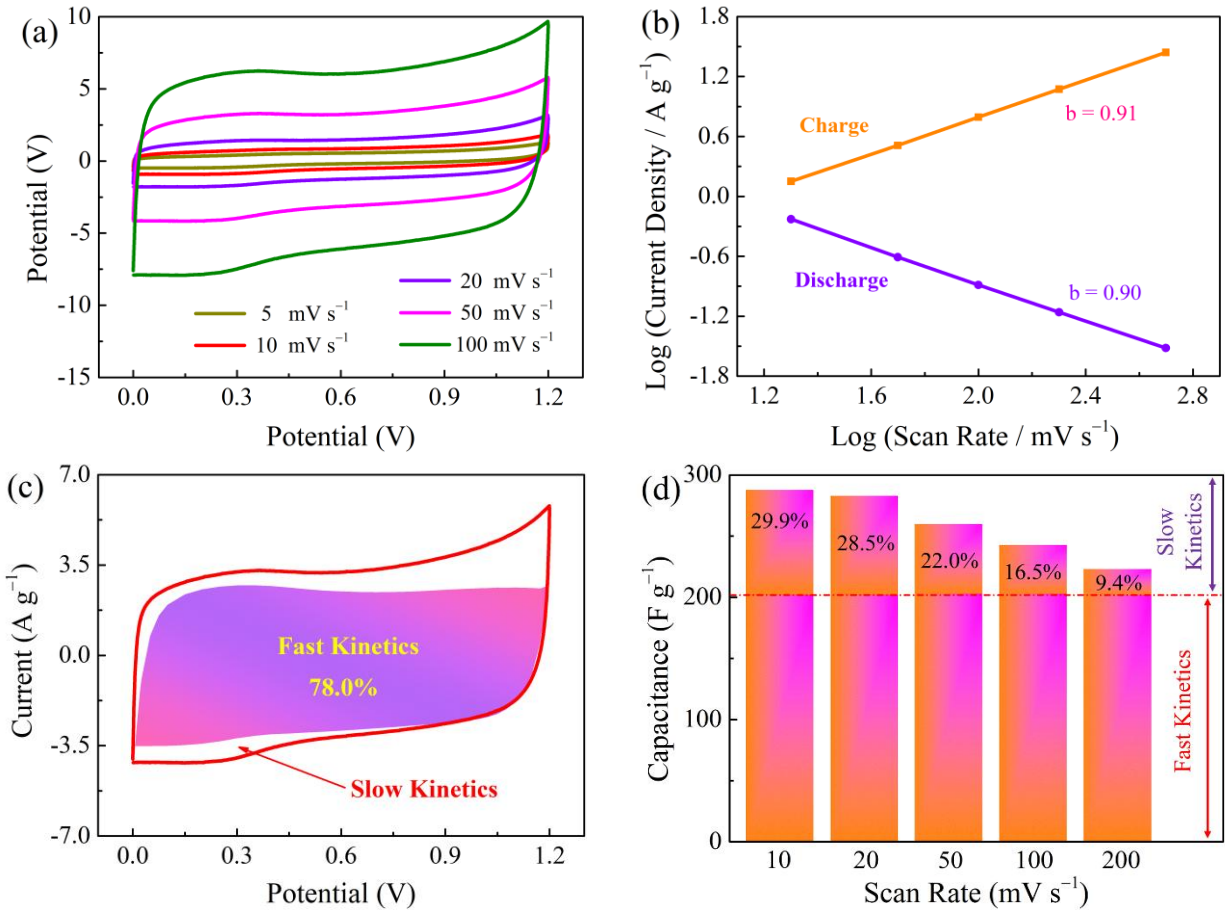

Fig. S15 (a) CV curves at various scan rates, (b) Absolute current density and scan rate obey the power law, $i=kv^b$, in charge/discharge process, (c) Decoupling of the capacitance contributed by the fast-kinetic process (shadow) and the slow-kinetic processes (blank), (d) Histograms of the capacitance contribution from fast and slow kinetic process of BQ/CD-C supercapacitor.

Table S3. The capacitances fitted by the area of CV profiles at different scan rates (mV s^{-1}), the rage of *b* value, and the capacitance (F g^{-1}**)** associated with fast-kinetic process of BQ/*X*-C electrode.

Samples	10	20	50	100	200	*b* value	Fast capacitance
BQ/ED-C-750	306	294	256	231	204	0.92	206
BQ/PD-C-750	368	350	329	310	289	0.94~0.95	286
BQ/DN-C-750	300	283	264	248	227	0.91	208
BQ/CD-C-750	288	283	260	243	223	0.90~0.91	202

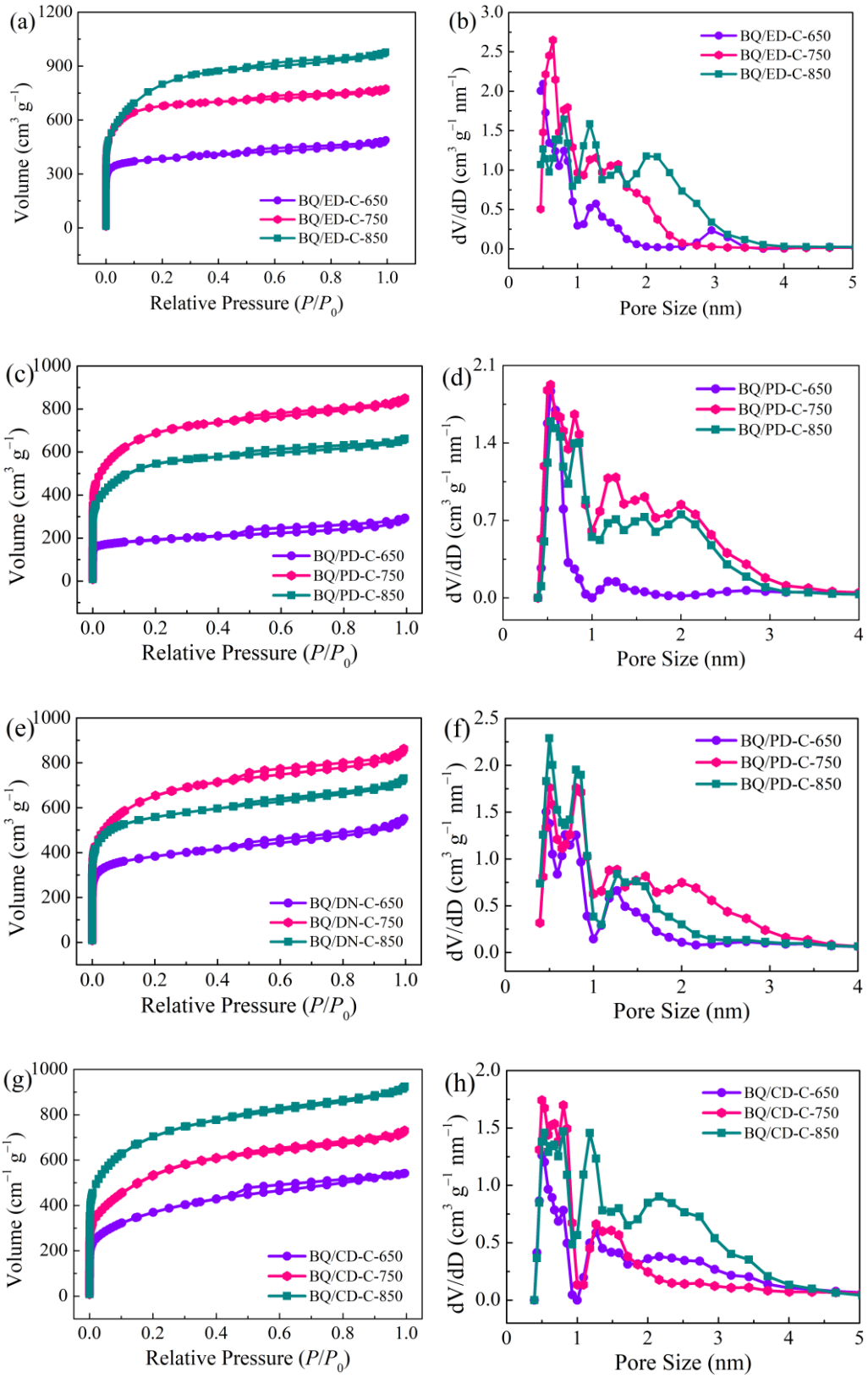

Fig. S16 N_2 sorption isotherms (a, c, e, and g) and pore size distribution curves (b, d, f, and h) of a, b) BQ/ED-C, (c, d) BQ/PD-C, e, f) BQ/DN-C, and (g, h) BQ/PD-C prepared at different heat-treatment temperatures.

Table S4. Pore structure parameters and elemental compositions of BQ/*X*-C.[a]

Samples	S_{BET} ($m^2\ g^{-1}$)	S_{Micro} ($m^2\ g^{-1}$)	V_{total} ($cm^3\ g^{-1}$)	N (wt.%)	O (wt.%)	*C* ($F\ g^{-1}$)	*E* ($Wh\ kg^{-1}$)
BQ/ED-C-650	1495	1369	0.75	6.83	9.17	235	11.8
BQ/ED-C-750	2524	2397	1.19	4.05	8.74	336	16.8
BQ/ED-C-850	2561	2359	1.51	2.75	7.14	282	14.1
BQ/PD-C-650	721	596	0.48	10.62	17.16	210	10.5
BQ/PD-C-750	2334	2111	1.31	5.16	8.28	363	18.2
BQ/PD-C-850	1823	1663	1.02	2.07	5.98	303	15.2
BQ/DN-C-650	1433	1202	0.84	7.49	17.73	252	12.6
BQ/DN-C-750	2183	1915	1.32	2.69	10.52	330	16.5
BQ/DN-C-850	2073	1817	1.12	1.67	9.68	291	14.6
BQ/CD-C-650	1203	921	0.84	2.80	19.08	278	13.9
BQ/CD-C-750	1732	1437	1.11	1.74	9.38	302	15.1
BQ/CD-C-850	2352	2021	1.42	2.92	7.80	311	15.6

[a] S_{BET}: surface area; S_{Micro}: micropore surface area; V_{total}: total pore volume.

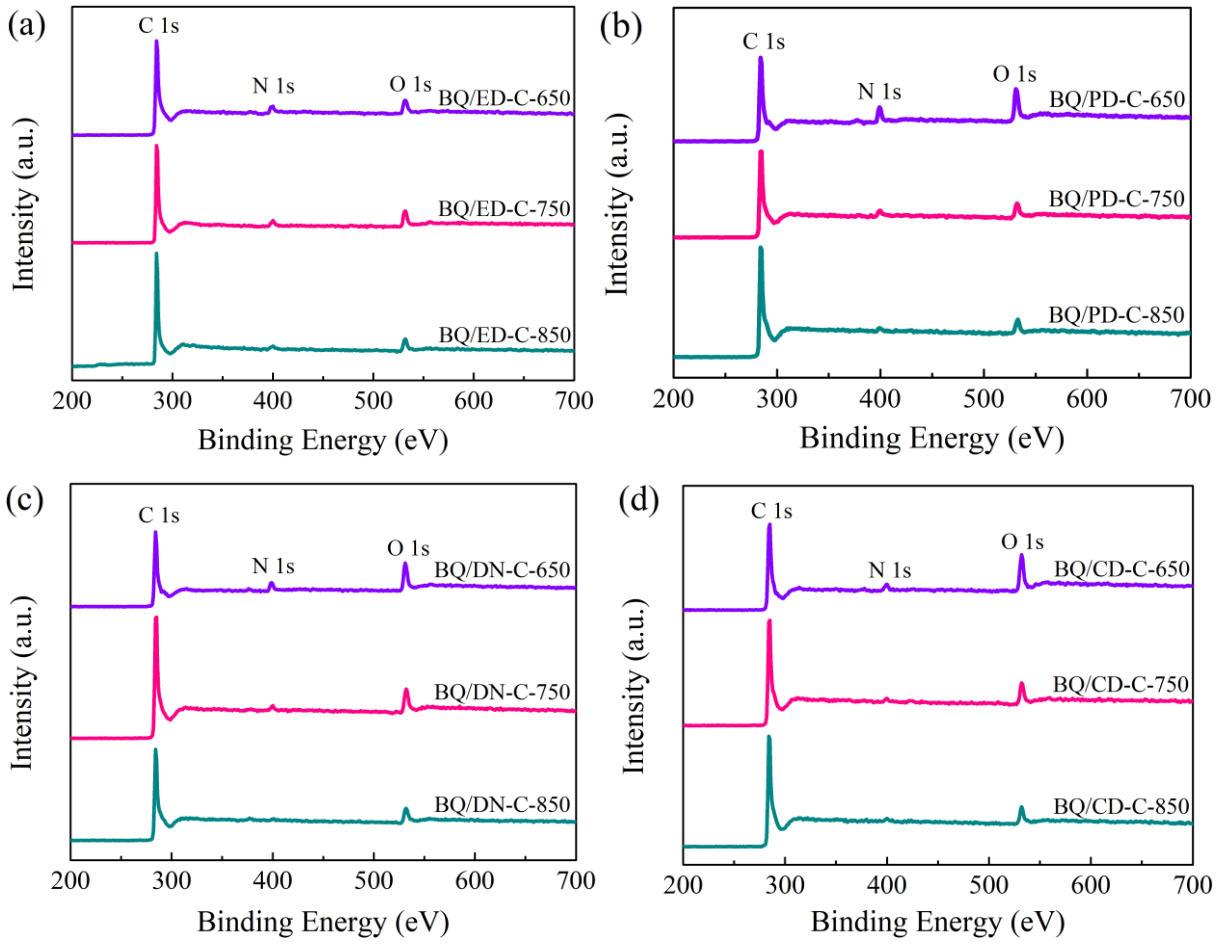

Fig. S17 XPS survey spectra of (a) BQ/ED-C, (b) BQ/PD-C, (c) BQ/DN-C, and (d) BQ/CD-C.

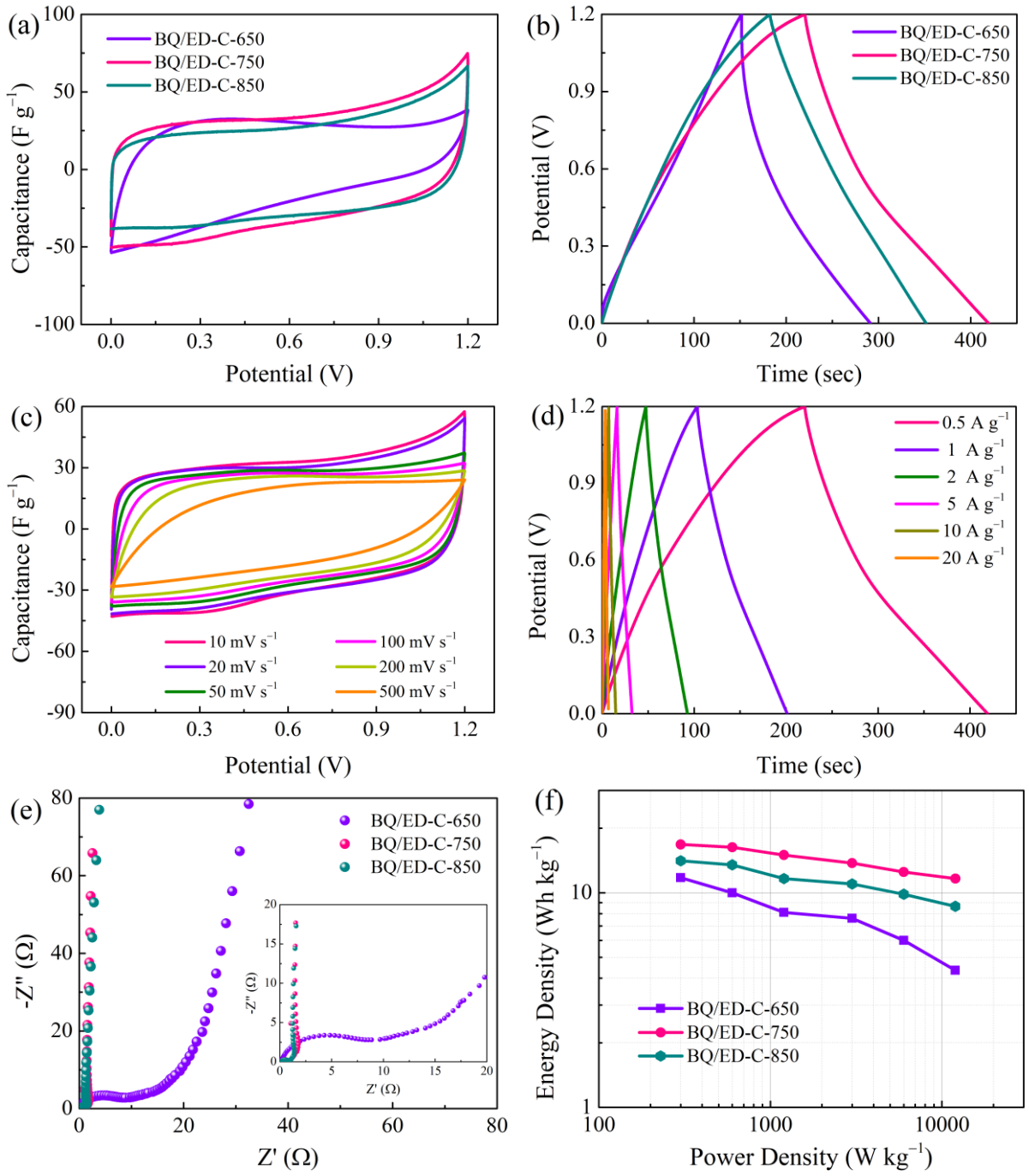

Fig. S18 (a) CV curves at 10 mV s^{-1} and (b) GCD curves at 0.5 A g^{-1} of BQ/ED-C-*Y* devices; (c) CV and (d) GCD profiles of BQ/ED-C-750 supercapacitor; (e) Nyquist plots and f) Ragone plots of BQ/ED-C-*Y* devices using 1 M H_2SO_4 electrolyte.

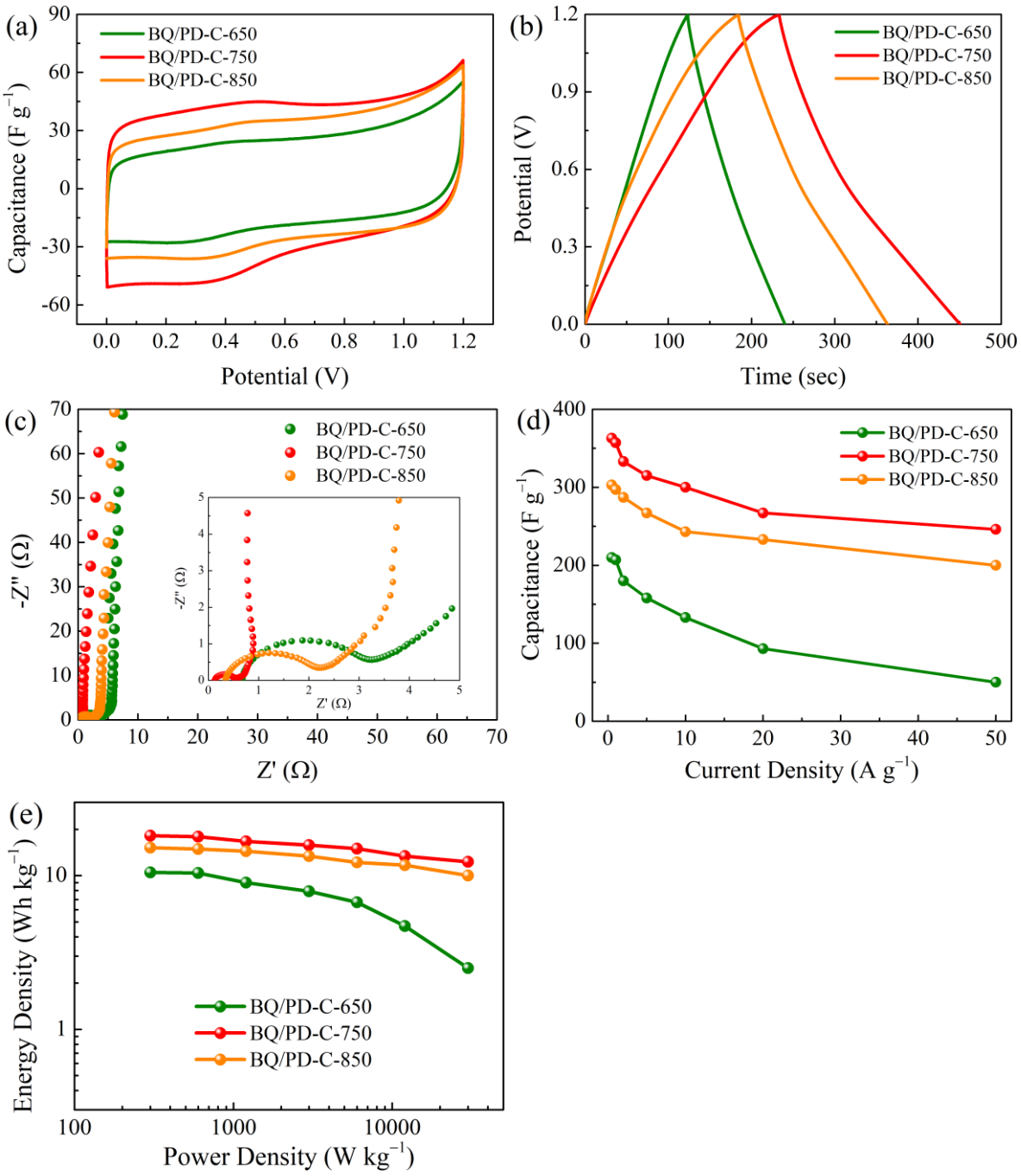

Fig. S19 (a) CV curves at 10 mV s^{-1}, (b) GCD curves at 0.5 A g^{-1}, (c) Nyquist plots, (d) Comparison of capacitance between the samples at various current densities, (e) Ragone plots of BQ/PD-C-*Y* devices using 1 M H_2SO_4 electrolyte.

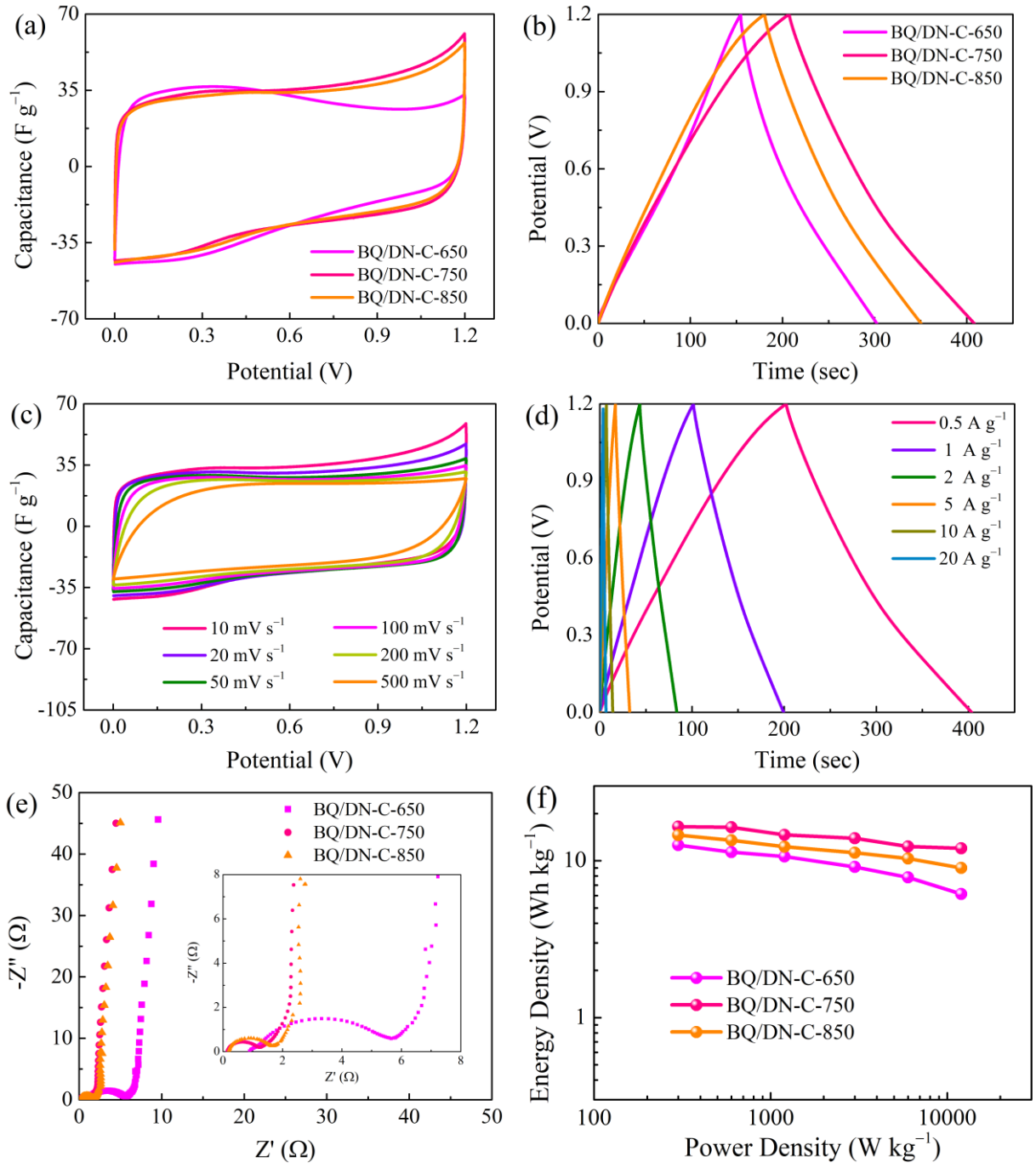

Fig. S20 (a) CV curves at 10 mV s^{-1} and (b) GCD curves at 0.5 A g^{-1} of BQ/DN-C-*Y* devices; (c) CV and (d) GCD profiles of BQ/DN-C-750 supercapacitor using 1 M H_2SO_4 electrolyte; (e) Nyquist plots and (f) Ragone plots of BQ/DN-C-*Y* devices.

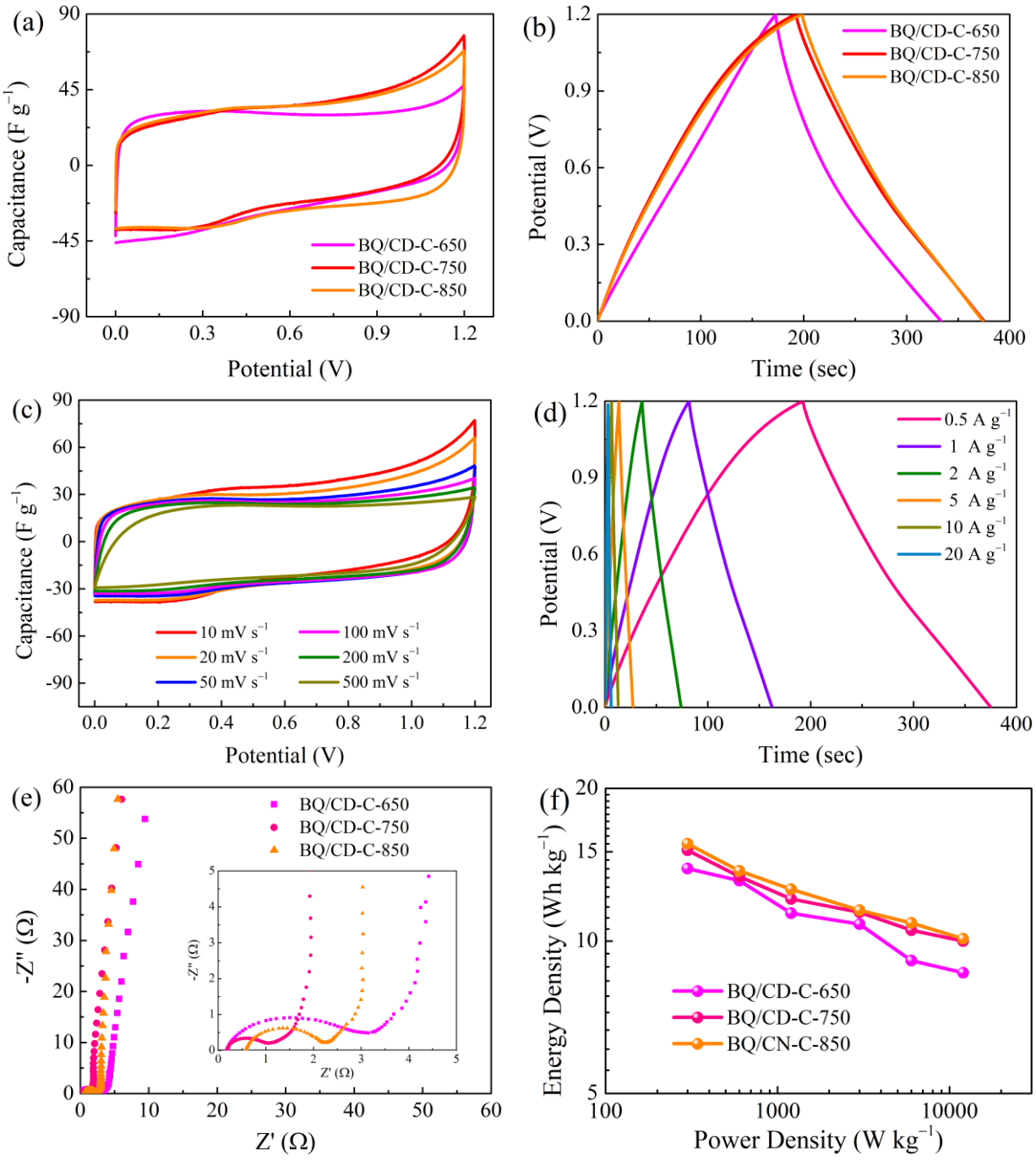

Fig. S21 (a) CV curves at 10 mV s^{-1} and (b) GCD curves at 0.5 A g^{-1} of BQ/CD-C-*Y* devices; (c) CV and (d) GCD profiles of BQ/CD-C-750 based supercapacitor using 1 M H_2SO_4 electrolyte; (e) Nyquist plots and (f) Ragone plots of BQ/CD-C-*Y* devices.

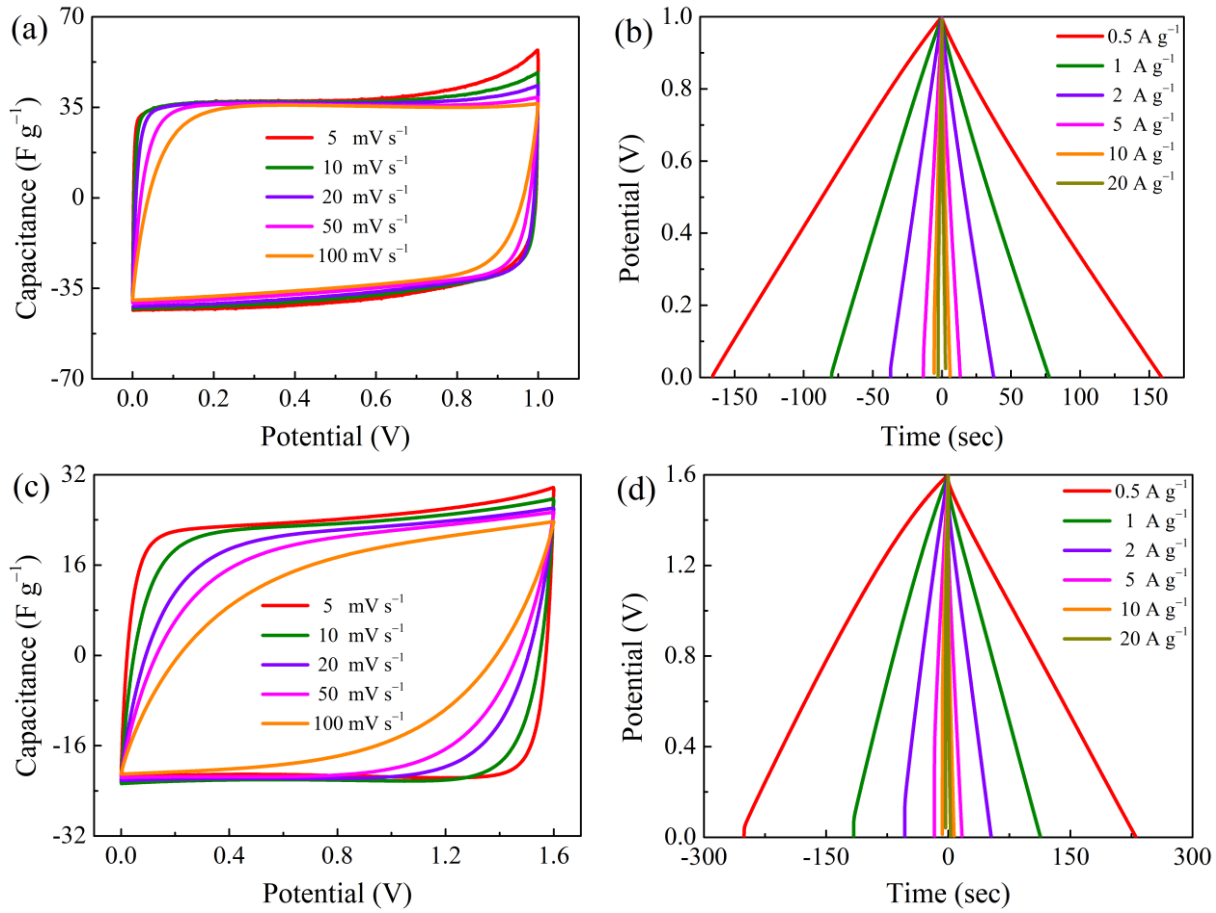

Fig. S22 CV curves and GCD profiles of the assmebled supercapcitors using (a, b) 6 M KOH electrolyte and (c, d) 1 M Na_2SO_4 electrolyte solution.

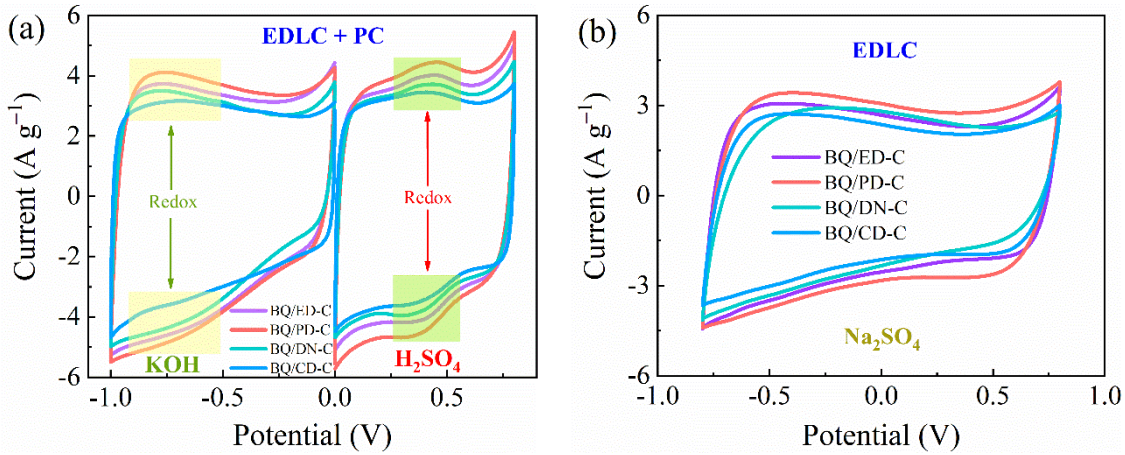

Fig. S23 CV curves of BQ/*X*-C electrodes tested in a three-electrode system using different electrolytes: (a) KOH and H_2SO_4 with electric double-layer capacitiance (EDLC) and pseudocapacitance (PC) contribution, and (b) Na_2SO_4 with only EDLC contribution.

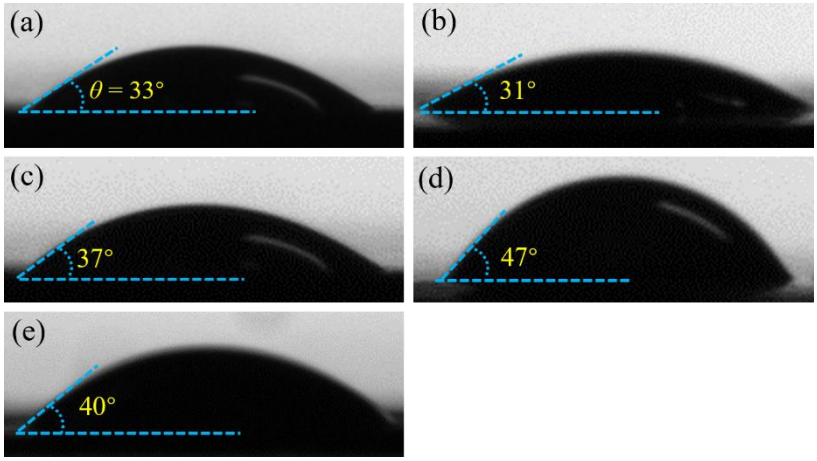

Fig. S24 The contact angles of (a) KOH, (b) Na_2SO_4, (c) LiTFSI, (d) $TEMABF_4$/PC, and (e) $EMIMBF_4$ electrolytes on the surface of BQ/PD-C.

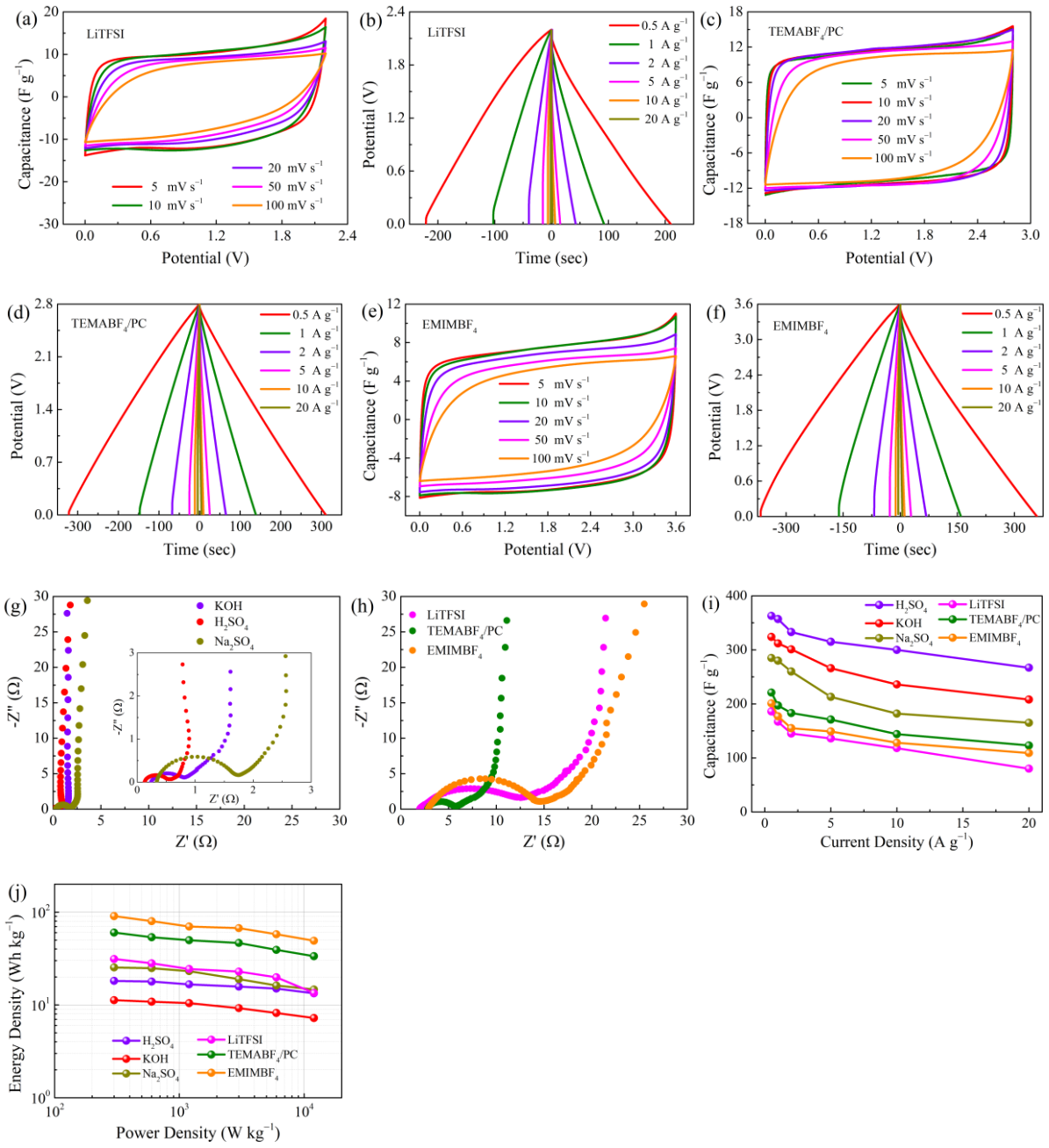

Fig. S25 CV and GCD profiles of the supercapcitors using (a, b) 7 m LiTFSI water-in-salt electrolyte, (c, d) 1 M TEMABF4/PC organic electrolyte, (e, f) EMIMBF4 ionic liquid electrolyte, (g, h) Nyquist plots, (i) capacitance *vs*. current density, and (j) Ragone plots.

References

1. H. Launay, C. M. Hansen and K. Almdal, *Carbon*, 2007, **45**, 2859−2865.
2. S. Ata, T. Mizuno, A. Nishizawa, C. Subramaniam, D. N.Futaba and K. Hata, *Sci. Rep.*, 2014,

4, 7232.

3. D. J. Hansen C., Kontogeorgis G., Panayiotou C., Willliams L., Poulsen T., Priebe H., Redelius P. , Boca Raton: CRC Press 2007.